Structure, Vol. 11, 1141–1150, September, 2003, ©2003 Elsevier Science Ltd. All rights reserved. DOI 10.1016/S0969-2126(03)00168-0

Crystal Structures of Substrate Complexes of Malic Enzyme and Insights into the Catalytic Mechanism

Xiao Tao, Zhiru Yang,[1] and Liang Tong*
Department of Biological Sciences
Columbia University
New York, New York 10027

Summary

Malic enzymes catalyze the oxidative decarboxylation of *L*-malate to pyruvate and CO_2 with the reduction of the NAD(P)$^+$ cofactor in the presence of divalent cations. We report the crystal structures at up to 2.1 Å resolution of human mitochondrial NAD(P)$^+$-dependent malic enzyme in different pentary complexes with the natural substrate malate or pyruvate, the dinucleotide cofactor NAD$^+$ or NADH, the divalent cation Mn^{2+}, and the allosteric activator fumarate. Malate is bound deep in the active site, providing two ligands for the cation, and its C4 carboxylate group is out of plane with the C1-C2-C3 atoms, facilitating decarboxylation. The divalent cation is positioned optimally to catalyze the entire reaction. Lys183 is the general base for the oxidation step, extracting the proton from the C2 hydroxyl of malate. Tyr112-Lys183 functions as the general acid-base pair to catalyze the tautomerization of the enolpyruvate product from decarboxylation to pyruvate.

Introduction

Malic enzyme (ME; EC 1.1.1.39) catalyzes the reversible oxidative decarboxylation of *L*-malate to pyruvate and CO_2 with the concomitant reduction of the cofactor NAD$^+$ or NADP$^+$ (Chou et al., 1994; Cleland, 2000; Hsu and Lardy, 1967; Loeber et al., 1991; Moreadith and Lehninger, 1984; Rao et al., 2000). The enzyme requires divalent cations (Mg^{2+}, Mn^{2+}, or others) in the catalysis of this reaction.

$$\text{NAD(P)}^+ + \textit{L}\text{-malate} \Leftrightarrow \text{NAD(P)H} + \text{pyruvate} + CO_2$$

ME activity was first isolated from pigeon liver (Ochoa et al., 1947) and has since been found in most living organisms, from bacteria to humans. Most MEs are homotetramers, with monomers containing ~550 amino acids and having molecular weights of ~60 kDa. The amino acid sequences of MEs are highly conserved across all the organisms, but they lack recognizable homology to other proteins, including other oxidative decarboxylases. The wide distribution of ME activity in nature and the high degree of sequence conservation are consistent with the important biological functions of these enzymes, such as photosynthesis in C4 plants and even some C3 plants (Hibberd and Quick, 2002) and biosynthesis of fatty acids and steroids in liver and adipose tissues in animals.

*Correspondence: tong@como.bio.columbia.edu
[1] Present address: Division of Biology, California Institute of Technology, Pasadena, California 91125.

In mammals, three isoforms of ME have been identified—cytosolic NADP$^+$-dependent ME (c-NADP-ME) (Chang et al., 1991; Loeber et al., 1994a), mitochondrial NADP$^+$-dependent ME (m-NADP-ME) (Loeber et al., 1994b), and mitochondrial NAD(P)$^+$-dependent ME (m-NAD-ME) (Loeber et al., 1991). m-NAD-ME can use both NAD$^+$ and NADP$^+$ as cofactor (dual specificity) but prefers NAD$^+$ under physiological conditions. It is believed that m-NAD-ME, via the NADH and pyruvate products, may have an important role in the metabolism of glutamine for energy production in rapidly proliferating tissues (e.g., spleen, thymus, and mucosal cells of small intestine) and tumors (McKeehan, 1982).

We have recently reported the crystal structures of human m-NAD-ME in both open and closed forms, in complex with NAD$^+$ or ATP, Mn^{2+}/Mg^{2+}, and various transition-state analog inhibitors (Xu et al., 1999; Yang et al., 2000a, 2000b, 2002a; Yang and Tong, 2000), as well as the structure of the pigeon c-NADP-ME (Yang et al., 2002b). The structure of the *Ascaris suum* m-NAD-ME in an open form has also been reported (Coleman et al., 2002). These studies establish ME as a new class of oxidative decarboxylases with a distinct backbone structure (Figure 1A). On the basis of the structures, the ME tetramer appears to be a dimer of dimers (Figure 1B), and each monomer can be divided into four domains, A–D. Domains A (residues 23–130) and D (residues 539–573) are mostly involved in the dimer and tetramer formation, whereas domains B (residues 131–277 and 467–538) and C (residues 278–466), together with several residues from domain A, are responsible for the catalysis by the enzyme. The structural information revealed the binding modes for NAD$^+$, NADP$^+$, Mn^{2+}, and the transition-state analog inhibitors, as well as the molecular mechanism for the regulation of m-NAD-ME by ATP and fumarate (Yang et al., 2002a).

To get a more complete understanding of the catalytic mechanism of these important enzymes, structural information on the binding modes of the genuine substrates of the enzyme, malate and pyruvate, are needed. We report here the crystal structure at 2.3 Å resolution of human m-NAD-ME in a pentary, nonproductive complex with NADH, *L*-malate, Mn^{2+}, and fumarate, as well as the structure at 2.1 Å resolution of the pentary complex with NAD$^+$, pyruvate, Mn^{2+}, and fumarate. As an independent observation for the binding mode of malate, we have also determined the structure at 2.3 Å resolution of m-NAD-ME in a pentary complex with ATP, malate, Mn^{2+}, and fumarate. These structures clearly define the binding modes for the substrate *L*-malate and pyruvate and confirm the binding modes for the divalent cation and cofactor NAD$^+$ as reported earlier. The structural information also helps to identify the general acid and general base in the catalysis by malic enzymes and shows that the divalent cation and the Lys183 residue play crucial roles in both steps of the reaction. Residue Tyr112, or, more appropriately, the Tyr112-Lys183 pair, functions as the general acid.

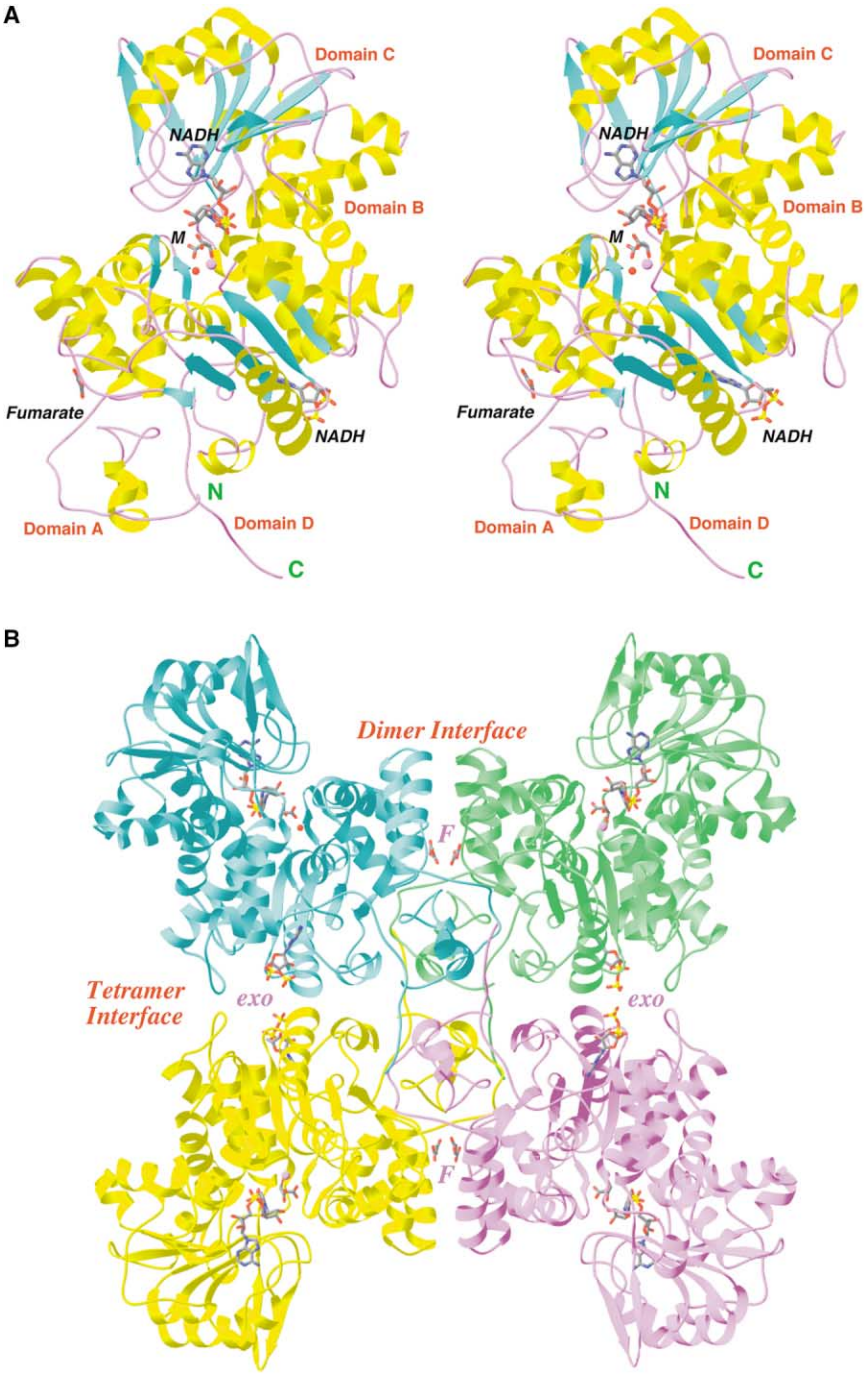

Figure 1. Structure of Human m-NAD-ME in Complex with NADH, *L*-Malate, Mn^{2+}, and Fumarate

(A) Schematic drawing of the monomer of human m-NAD-ME. β strands, cyan; α helices, yellow; connecting loops, purple. The NADH molecule in the active site, the ADP portion of the NADH molecule in the exo site, malate (*M*), and fumarate are shown as stick models, colored in gray for carbon atoms. The Mn^{2+} ion and its liganding water are shown as pink and red spheres, respectively.

(B) Schematic drawing of the tetramer of the enzyme. The monomers are colored in cyan, green, yellow, and purple, respectively. The fumarate molecules are in the dimer interface (*F*). This figure was produced with Ribbons (Carson, 1987).

Results and Discussion

Overall Structure

The crystal structures of human m-NAD-ME in three different pentary complexes, containing the substrate *L*-malate (MAL) or pyruvate (PYR), have been determined at up to 2.1 Å resolution (Table 1). As was observed with the oxalate (OXL) complex (Yang et al., 2000b), the enzyme is in a closed form in the current structures (Figure 1A). There is a tetramer of the enzyme

Table 1. Summary of Crystallographic Information

Complex (in addition to Mn^{2+}/fumarate)	Malate/NADH	Pyruvate/NAD	Malate/ATP
Cell parameters (a, b, c, β)	227.3, 117.3, 113.0, 109.8	225.8, 117.1, 111.8, 109.6	226.1, 117.3, 111.3, 109.0
Maximum resolution (Å)	2.3	2.1	2.3
Number of observations	363,991	420,965	379,634
R_{merge} (%)[a]	8.3	8.1	8.6
Resolution range for refinement	20–2.3	20–2.1	20–2.3
Number of reflections	116,154	144,535	112,846
Completeness (%)	94	91	93
R factor (%)[b]	20.5	19.2	21.1
Free R factor (%)	25.6	23.6	25.2
Rms deviation in bond lengths (Å)	0.007	0.006	0.007
Rms deviation in bond angles (°)	1.3	1.3	1.3

[a] $R_{merge} = \sum_h \sum_i |I_{hi} - \langle I_h \rangle| / \sum_h \sum_i I_{hi}$

[b] $R = \sum_h |F_h^o - F_h^c| / \sum_h F_h^o$

in the crystallographic asymmetric unit (Figure 1B). The four monomers have similar conformations, with a root-mean-square (rms) distance of ~0.3 Å between the 553 equivalent Cα atoms of any pair of monomers in each structure. The tetramers maintain almost perfect 222 point group symmetry; thus, each monomer has essentially the same environment in this oligomer.

The crystals studied here are isomorphous to that of the OXL complex (Yang et al., 2000b), and the overall structures of the monomers are similar to that in the OXL complex. In addition, there are only small differences in the organization of the dimers and tetramers of these two different complexes, with a rms distance of about 0.4 Å when all 2212 Cα atoms of any pair of the two tetramers are superimposed. This structural similarity validates our earlier descriptions of the active site conformation of the enzyme based on structures in complex with transition-state analog inhibitors.

As we reported previously, there are two binding sites for the cofactor (NAD^+ or NADH) or ATP in each monomer of the enzyme (Figure 1A). The interactions between the enzyme and NAD^+/NADH or ATP in the exo site are essentially the same as those observed earlier (Yang et al., 2002a; Yang and Tong, 2000). Similarly, the allosteric activator fumarate is bound in the current structures, and its interactions with the enzyme are essentially the same as those observed before (Yang et al., 2002a). These interactions will not be described further in this paper.

Binding Mode of Substrate *L*-Malate

In the NADH/MAL/Mn^{2+}/fumarate pentary complex, *L*-malate is bound deep in the active site pocket (Figure 2A), with its C2 hydroxyl group and one of its C1 carboxylate oxygen atoms as ligands to the divalent cation (Figure 2B). Besides interactions with the metal ion, there is a large network of hydrogen-bonding and ionic interactions between MAL and the enzyme (Figures 2A and 2B). The C1 carboxylate group of MAL shows monodentate ionic interactions with the side chain guanidinium group of Arg165, using the same oxygen atom (O1A) that is ligated to the divalent cation (Figure 2B). Some conformational variability was observed for this side chain between the four monomers of the tetramer. The other carboxylate oxygen atom (O1B) is within hydrogen-bonding distance to the side chain amide of Asn421 and the 2′-hydroxyl of the nicotinamide ribose.

The C4 carboxylate group is positioned such that it is out of the plane defined by the C1, C2, O2 and C3 atoms of MAL (Figures 2A and 2B). This carboxylate has hydrogen-bonding interactions with the side chain of Asn466, the water ligated to the cation, and a second water molecule (Figures 2A and 2B). In contrast, the C3 atom of MAL does not have close contacts with atoms in the enzyme, with the shortest distance being about 3.3 Å to the side chain of Asn466 (Figure 2B).

An Independent Observation of Malate Binding Mode in the ATP/Malate Complex

Our structure of the NADH/MAL/Mn^{2+}/fumarate pentary complex represents a nonproductive state of the enzyme. There are concerns as to whether the binding mode of MAL observed in this complex could have been adversely affected by the NADH molecule. Our repeated attempts at obtaining the structure of the productive, Michaelis complex of malic enzyme with NAD^+ and MAL were unsuccessful.

As an independent observation for the binding interactions of MAL, we determined the crystal structure of the ATP/MAL/Mn^{2+}/fumarate pentary complex (Table 1). The active site near the MAL molecule has a cavity in this structure, because of the absence of the nicotinamide ring (Figure 3). Nonetheless, the position of MAL in this active site is essentially identical to that observed in the NADH/MAL complex. This confirms that the binding mode of MAL observed in these two structures is likely to correspond to that in the natural substrate complex. A difference in the binding mode of the cofactor is observed (Figure 3), and this will be discussed below.

Binding Mode of Pyruvate

In the NAD^+/PYR/Mn^{2+}/fumarate pentary complex, the pyruvate molecule is bound with its plane parallel to, and about 3.4 Å from, that of the nicotinamide ring of NAD^+, suggesting possible π-π interactions (Figure 4). The oxidative decarboxylation of MAL by ME produces both PYR and carbon dioxide. To define the binding mode of the latter, we included 10 mM bicarbonate in the

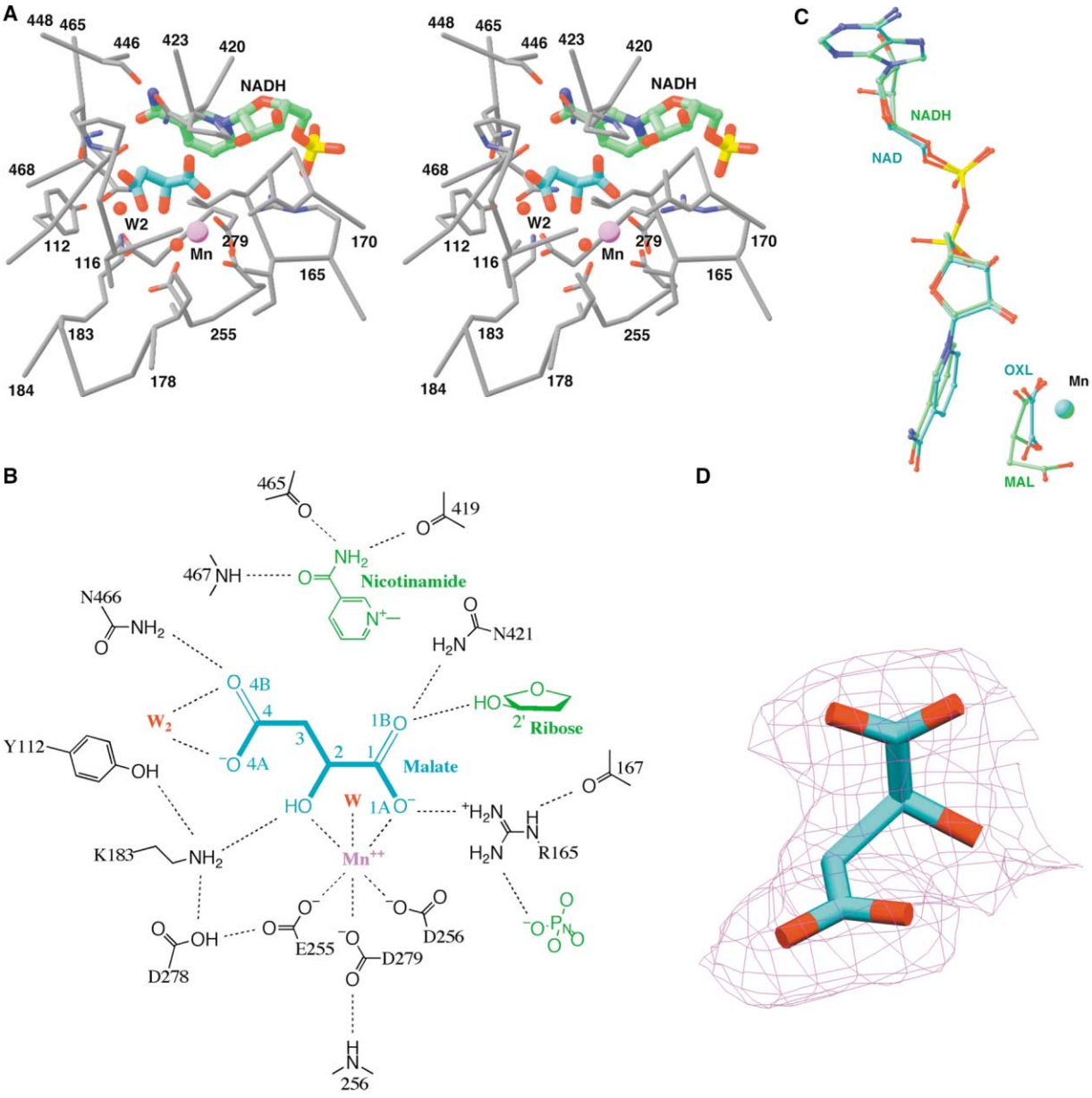

Figure 2. Binding of Malate to the Active Site

(A) Stereo diagram showing the binding of malate (cyan for carbon atoms) to the active site (gray for carbon atoms). The nicotinamide ribose portion of NADH (green) is also shown.

(B) Schematic drawing showing the hydrogen-bonding interactions between malate and the enzyme in the active site.

(C) Schematic drawing showing the comparison of binding modes of NADH/malate (green for carbon atoms) and NAD^+/oxalate (cyan) to the enzyme.

(D) Final $2F_o - F_c$ electron density map at 2.3 Å resolution for the malate molecule in the active site. The contour level is at 1 σ. (A) and (C) were produced with Ribbons (Carson, 1987), and (D) was produced with Setor (Evans, 1993).

crystallization solutions. However, we did not observe electron density for this group or CO_2 in the structural analysis at 2.1 Å resolution. It is clear there is a cavity near the C3 atom of PYR that could accommodate the CO_2 molecule (Figure 4). Further experiments are needed to define the interactions between CO_2 and the enzyme.

The binding mode of PYR is essentially the same as that of OXL (Yang et al., 2000b), with one of the largest differences being a 0.3 Å shift in the position of the C2 atom (Figure 4). In contrast, MAL shows much larger differences in the positions of its atoms relative to OXL or PYR, especially at the C2 position (Figure 2C and see below).

Binding Modes of NAD^+ and NADH

The position of the NAD^+ molecule in the NAD^+/PYR complex is identical to that in the NAD^+/OXL complex (Yang et al., 2000b), suggesting that this is likely the

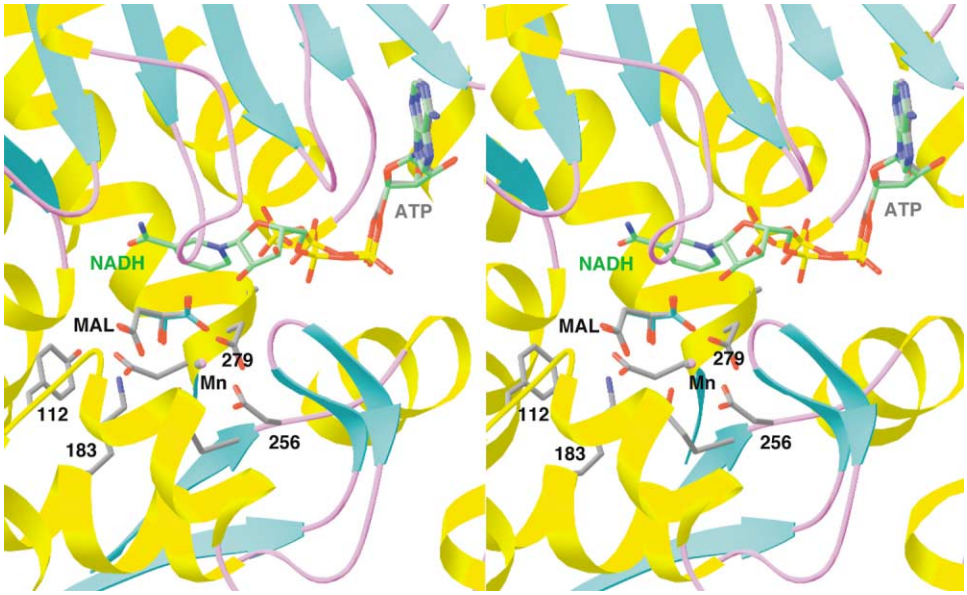

Figure 3. Binding Mode of Malate in the ATP/Malate Complex

Stereo diagram showing the active site of m-NAD-ME in complex with ATP and malate (both gray for carbon atoms). Also shown is the binding mode of NADH (green) and malate (cyan) in the NADH/malate complex. This figure was produced with Ribbons (Carson, 1987).

natural binding mode for NAD^+ to the enzyme (Figure 4). In contrast, the nicotinamide ring in the NADH/MAL complex assumes a somewhat different conformation, which gives rise to a shift of about 0.6 Å in the position of the C4 atom, away from the substrate MAL (Figure 2C). This difference may be a consequence of the reduction of NAD^+ or the steric repulsion between MAL and NADH in the dead end complex.

The proton on the C2 atom of MAL is pointed toward the C4 atom of the nicotinamide ring, with a hydride transfer distance of about 2 Å for the conformation of NAD^+ in the NAD^+/PYR complex. As discussed earlier, this binding mode of MAL clearly explains the stereospecificity of the enzyme for *L*-malate and for the A face of NAD^+ (Xu et al., 1999; Yang et al., 2000b).

The General Base for the Dehydrogenation Step

The catalysis by malic enzymes generally proceeds in three steps—dehydrogenation (oxidation) of malate to produce oxaloacetate, decarboxylation of oxaloacetate to produce enolpyruvate, and, finally, tautomerization of enolpyruvate to produce pyruvate (Figures 5A–5E) (Cleland, 1999). On the basis of kinetic and mutagenesis studies, Asp279 has been proposed as the general base,

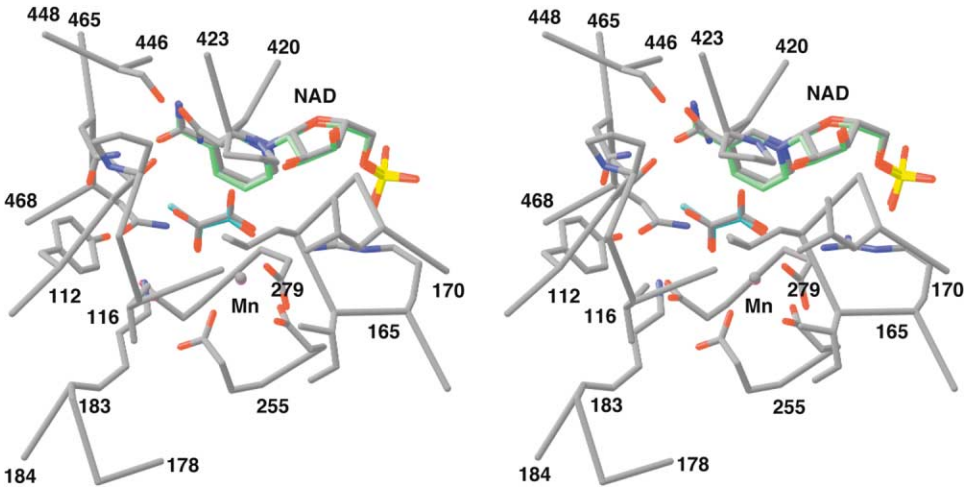

Figure 4. Binding of Pyruvate to the Active Site

Stereo diagram showing the binding of pyruvate (cyan for carbon atoms) to the active site (gray for carbon atoms). The nicotinamide ribose portion of NADH (green) is also shown. The binding mode of NAD^+ and oxalate (both in gray) in the NAD^+/oxalate complex is shown, as well. This figure was produced with Ribbons (Carson, 1987).

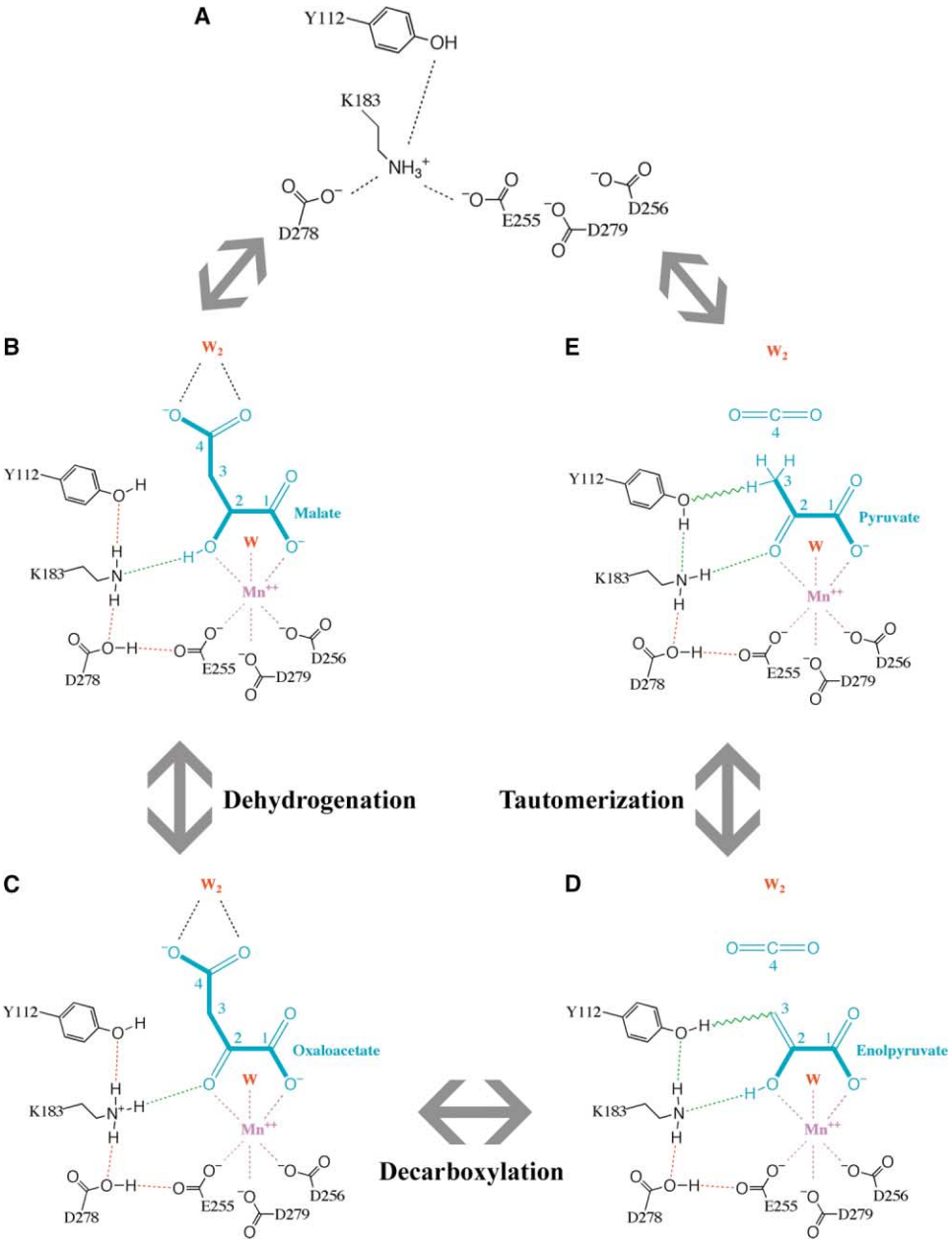

Figure 5. Proposed Catalytic Mechanism of Malic Enzyme, Showing Various Steps along the Reaction Pathway

Hydrogen bonds are shown as dotted red lines or as dotted green lines if a proton transfer is involved during that step of the reaction. The proton transfer between Tyr112 and the C3 atom of (enol)pyruvate is indicated by the wavy green line.

(A) Before substrate binding, with the enzyme in an open form.

(B) After malate binding, with the enzyme in a closed form and Lys183 in the neutral form, ready to extract the proton from the C2 hydroxyl.

(C) After malate is oxidized to oxaloacetate.

(D) After the decarboxylation reaction. Tyr112 is poised to protonate the C3 atom.

(E) After the tautomerization to pyruvate.

which extracts the proton from the C2 hydroxyl of MAL to initiate the dehydrogenation step (Karsten et al., 1999). Lys183 is proposed to be the general acid, protonating the enolpyruvate intermediate at the C3 position to initiate the tautomerization to pyruvate (Liu et al., 2000).

Our structure of m-NAD-ME in complex with the genuine substrate MAL allows us to assess these observations from the kinetic and mutagenesis experiments. Asp279 is a ligand to the metal ion, but it is not oriented correctly to extract the proton from the C2 hydroxyl of MAL (Figure 6A). In addition, the side chain is more than 3.4 Å away from the C2 hydroxyl. This side chain could undergo a conformational change to initiate the reaction, but such a change will not shorten the distance to the C2 hydroxyl. Moreover, this side chain is also hydrogen

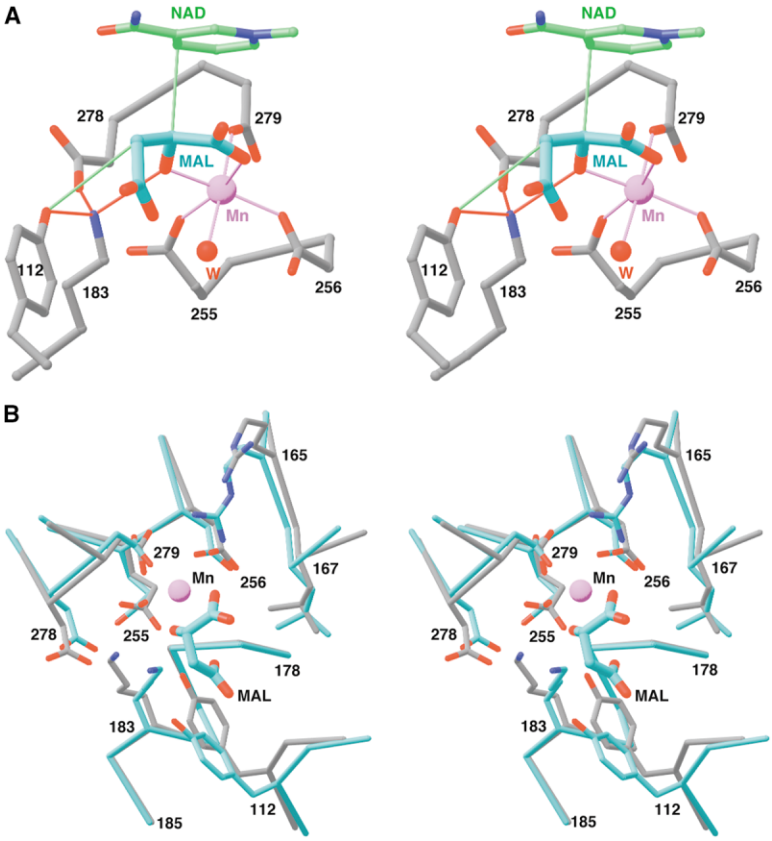

Figure 6. The Active Site of the Enzyme

(A) Stereo diagram showing the catalytic residues of the enzyme and the ligands of the cation. The hydrogen bonds for the ammonium ion of Lys183, red; the proton transfer from the C2 and C3 atoms of the substrate, green.

(B) Stereo diagram comparing the conformation of residues in the active site in the open (gray for carbon atoms) and closed (cyan) forms. Note the large changes in the side chains of Tyr112, Lys183, and Asp278.

bonded to the main chain amide of Asp256 (Figure 2B), making a conformational change less likely. Furthermore, such a change and the resulting protonation after proton transfer would, in all likelihood, disrupt the interactions with the cation. Therefore, the structural information suggests that Asp279 is probably not the general base of the reaction.

The importance of Asp279 for catalysis is more likely due to an indirect effect, that is, its ligating of the cation. Mutation of this residue to Glu in pigeon ME produced a 3,000-fold increase in the K_d for Mn^{2+} but only a small effect on V_{max} (Wei et al., 1995). Mutation of this residue to Ala in *Ascaris suum* ME lowered the affinity for the cation by such an extent that the substrate MAL must bind first to the enzyme (Karsten et al., 1999), which would then provide two ligands for binding the cation. This mutation also led to a 10,000-fold reduction in the V_{max}, in contrast to observations on the pigeon ME. This could be explained by the fact that the Ala side chain could not maintain the intricate hydrogen-bonding network in the active site (Figure 2B), which is crucial for the proper placement of the catalytic residues.

If Asp279 is not the general base, which group in the enzyme:substrate complex can extract the proton from the C2 hydroxyl? Our structure shows that the side chains of Lys183 and Asn467, as well as the water molecule bound to the cation, are within hydrogen-bonding distance to the C2 hydroxyl of MAL. This water molecule is, however, unlikely to function as the general base, as it is expected to have a very low pK_a value (below -1). Therefore, this leaves the Lys183 residue, which is perfectly positioned to extract the proton (Figure 6A), as the most likely candidate for the general base in the dehydrogenation reaction.

Mutation of the Lys183 residue has large effects on the catalytic activity of MEs (Kuo et al., 2000; Yang et al., 2000b). Mutation of this Lys to Ala in the *Ascaris suum* ME gave rise to a 130,000-fold decrease in the V_{max} of the overall reaction (Liu et al., 2000). Moreover, the mutant favors the decarboxylation of the oxaloacetate intermediate, while the wild-type enzyme favors the reductive hydrogenation reaction. It was suggested that the decarboxylation reaction is more suppressed in the wild-type enzyme by the Lys side chain (Liu et al., 2000). However, another explanation is that the Lys → Ala mutant cannot catalyze the hydrogenation reaction, because it cannot function as the general acid for the reverse (reduction) reaction.

For Lys183 to function as the general base, it needs to be in the neutral state at the start of the reaction (Figure 5B). Lys183 is hydrogen bonded to Asp278 in all the steps of the reaction. Asp278 is, in turn, hydrogen bonded to Glu255 when the substrate is present (Figures 5B–5E). As Glu255 is a ligand to the cation, the structure suggests that Asp278 is likely to be protonated to maintain this close contact with Glu255 (Figure 5B–5E), which would make it more likely for the Lys183 side chain to achieve a neutral state and be competent for catalysis. In the open form of the structure, before the binding of substrates, Lys183 is placed between Asp278 and Glu255 (Figure 6B) (Xu et al., 1999). In the structure of the open form of *Ascaris suum* ME, the Lys residue is

positioned at a similar location (Coleman et al., 2002). Upon substrate binding and the closure of the active site, the side chains of Lys183, Asp278, and Tyr112 undergo large conformational changes, bringing Asp278 and Glu255 into close proximity (Figure 6B) (Yang et al., 2000b).

Asp278 is strictly conserved among all malic enzymes, except in the α subunit of the enzyme from the plant *Amaranthus hypochondriacus*, where it is changed to Val and Tyr112 is changed to Ser (Long et al., 1994). Mutation of this Asp residue in *Ascaris suum* ME led to a 600-fold decrease in the k_{cat} of the enzyme (Karsten et al., 1999). The effect of mutating this residue in human m-NAD-ME is somewhat smaller, with about a 100-fold reduction in the V_{max} of the enzyme (data not shown). Therefore, Asp278 has a relevant, but not crucial, role in the catalysis by malic enzyme, despite its high degree of conservation. Other factors may also be important in stabilizing the Lys183 side chain in the neutral form in the substrate complex.

The General Acid for the Tautomerization Step

For the decarboxylation reaction, the enzyme binds MAL such that its C4 carboxylate group is out of the plane of the C1-C2-C3 atoms (Figure 6A). This may favor the decarboxylation of the oxaloacetate intermediate and contrasts with malate dehydrogenase, where MAL is bound with C4 in the same plane as the C1-C2-C3 atoms (Cleland, 1999). At the same time, the π electrons of this carboxylate group are likely not positioned optimally for decarboxylation, as otherwise the overall reaction would likely become concerted. This step of the reaction is catalyzed by the divalent cation functioning as a Lewis acid. In addition, Lys183 functions as a general acid, protonating the C2 hydroxyl to produce the neutral enol (Figure 5C).

For the tautomerization from enolpyruvate to pyruvate, a general acid is needed to protonate the enolpyruvate intermediate at the C3 position, and a general base is needed to extract the proton from the C2 hydroxyl (Figure 5D). Lys183 was proposed as the general acid on the basis of kinetic and mutagenesis studies (Liu et al., 2000). However, the distance between the ammonium ion of Lys183 and the C3 atom of PYR is more than 3.6 Å. Considering the fact that our observations are based on a nonproductive, dead end complex, we cannot completely exclude the possibility that the binding mode of PYR and/or the conformation of active site residues are different in the reactive complex, thereby allowing Lys183 to function as the general acid. However, we believe such a possibility is unlikely because of the large number of hydrogen-bonding interactions for the ammonium ion of Lys183 (Figure 6A). Moreover, Lys183 needs to function as the general base in this reaction, extracting the proton from the C2 hydroxyl (Figure 5D).

Our structure suggests that Tyr112 is the general acid for this reaction, as it is the only close neighbor of the C3 atom in the PYR complex, with a distance of 3.1 Å (Figure 4). Moreover, Tyr112 and Lys183 are hydrogen bonded to each other, so these two residues function as a general acid-base pair, in concert with each other, to catalyze the tautomerization of enolpyruvate to pyruvate. In this mechanism, Tyr112 donates its hydroxyl proton to the C3 atom, while accepting a proton from the side chain of Lys183 (Figure 5D). Concomitantly, Lys183 extracts the proton from the C2 hydroxyl of the intermediate. This maintains both Tyr112 and Lys183 in the neutral form (Figure 5E).

Mutation of this Tyr residue to Phe gave rise to about a 1500-fold decrease in the k_{cat} for the oxidative decarboxylation of malate (Liu et al., 2000; Yang et al., 2000b). The smaller effect, as compared to that from the mutation of Lys183, could be explained if the protonation of enolpyruvate is not a rate-determining step of the forward reaction. It may also be possible that a water molecule is recruited into the active site in the Tyr → Phe mutant, which partially rescues the catalytic activity of the mutant. It would be interesting to determine the structure of this mutant, as well as the effect of this mutation on the rate of the reverse reaction.

The Lys → Ala mutant in *Ascaris suum* ME cannot catalyze the exchange of the methyl protons of PYR with solvent (Liu et al., 2000). This was interpreted to mean that Lys183 is the general acid for the decarboxylation reaction. Our mechanism suggests instead an alternative explanation, as the mutation disrupts the Tyr112-Lys183 general acid-base pair. For the enolization of PYR, Lys183 is required as a general acid to protonate the C2 carbonyl. Without the Lys side chain, Tyr112 cannot function as the general base to extract the proton from the C3 atom of PYR. It was also observed kinetically that the Tyr → Phe mutation does not affect the partition ratio of oxaloacetate into malate or pyruvate (Liu et al., 2000). This may not, however, contradict the role of Tyr112 as the general acid. If the decarboxylation of oxaloacetate is the committed step in the conversion to pyruvate, the protonation by Tyr112 occurs after the decarboxylation and may not affect the partition ratio.

Implications for the Catalytic Mechanism

All the residues that show interactions with MAL and PYR are highly conserved among the malic enzymes, suggesting their importance in substrate binding and/or catalysis by these enzymes. On the basis of our structural analyses and generally supported by the mutagenesis and kinetic studies, we propose the following model for the reaction cycle of malic enzymes.

(1) Before substrate binding, the enzyme is in an open form, where Lys183 is placed between the side chains of Tyr112, Asp278, and Glu255 (Figures 5A and 6B).

(2) Upon binding of the substrate MAL and the divalent cation, the enzyme undergoes a large conformational change, causing the closure of the active site. In this process, the side chain of Lys183 moves by about 2 Å in order to hydrogen bond to the C2 hydroxyl of MAL (Figure 6B).

In the substrate complex, the hydrogen-bonding partners of Lys183 are Tyr112, Asp278, and the C2 hydroxyl of MAL (Figures 5B and 6A). The side chain of Tyr112 moves by 3.3 Å and that of Asp278 moves by 1.7 Å to stay hydrogen bonded to Lys183.

(3) Lys183 functions as the general base and extracts the proton from the C2 hydroxyl group of MAL, and the

divalent cation may also have an important role in this process. At the same time, the C2 proton is transferred to the C4 position of $NAD(P)^+$ as a hydride. MAL is converted to oxaloacetate (Figure 5C).

The dehydrogenation reaction changes the hybridization state of the C2 atom of the substrate from sp^3 to sp^2. Comparisons of the binding modes of MAL, PYR, and OXL suggest that the C2 atom may move by about 0.6 Å in this process (Figure 2C). This change in hybridization is also expected to reduce the C2-C3-C4 bond angle of the substrate, which may also facilitate the decarboxylation reaction (Cleland, 1999).

(4) The oxaloacetate intermediate is then decarboxylated to produce the enolpyruvate intermediate and carbon dioxide (Figure 5D). This reaction is facilitated by the fact the C4 carboxylate group is out of the plane of the C1-C2-C3 atoms when bound to the enzyme. In addition, the metal ion has an important role in this reaction, as well, polarizing the C2 carbonyl of oxaloacetate. Lys183 acts a general acid in this reaction, transferring its proton back to the substrate to produce the neutral enol (Figure 5D).

The hydration of the CO_2 product is likely to be slow, even in the presence of a water molecule nearby (W_2) in the active site. Kinetic studies show that CO_2, rather than bicarbonate, is the substrate for the reverse reaction (Mallick et al., 1991).

(5) Residues Tyr112 and Lys183 function as a general acid-base pair to catalyze the tautomerization of enolpyruvate to pyruvate, protonating enolpyruvate at the C3 position and deprotonating it at the C2 hydroxyl. This step requires the concerted movement of three protons—one from Tyr112 to C3, one from Lys183 to Tyr112, and one from the C2 hydroxyl to Lys183 (Figures 5D and 5E).

(6) After the completion of the reaction, the enzyme undergoes a conformational change to the open form, releasing the products of the reaction and restoring the protonation state of Lys183 (Figure 5A).

The proposed mechanism is fully reversible. By changing the directions of proton flow, PYR can be reductively carboxylated to produce MAL. The Lys183-Tyr112 pair is in the neutral form throughout the reaction in the presence of substrate, except in the oxaloacetate complex, where Lys183 carries a positive charge. The proton shared between these two residues shifts its position to keep both residues neutral in the other complexes.

In summary, we have determined the crystal structures of human mitochondrial $NAD(P)^+$-dependent malic enzyme in pentary complexes with the substrate *L*-malate or pyruvate. The structural information allows us to identify Lys183 as the general base that extracts the proton from the C2 hydroxyl of MAL for the dehydrogenation reaction and Tyr112-Lys183 as the general acid-base pair that catalyzes the tautomerization of the enolpyruvate intermediate after decarboxylation. The divalent cation is optimally positioned to help catalyze the entire reaction, explaining its requirement by malic enzymes. The mechanistic importance of the residues in the active site is consistent with, and supported by, the large body of kinetic and mutagenesis data on these enzymes.

Experimental Procedures

Protein Expression, Purification, and Crystallization

The protocols for expression and purification of human m-NAD-ME have been described previously (Bhargava et al., 1999; Loeber et al., 1991). In brief, m-NAD-ME (containing selenomethionyl residues) was overexpressed in *E. coli* and purified by anion exchange, ATP affinity, and gel filtration chromatography. Crystals were grown at 4°C by the hanging drop vapor diffusion method. The protein was at a concentration of 8 mg/ml, in a solution containing 30 mM Tris (pH 7.4), 30 mM KCl, 2 mM DTT, 10 mM NAD^+, NADH, or ATP, 5 mM $MnCl_2$, 5 mM fumarate, and 10 mM *L*-malate or pyruvate and bicarbonate. The reservoir solution contained 100 mM Bis-Tris (pH 6.0–7.0), 12%–15% (w/v) PEG 3350, and 0.1 M *L*-malate or 0.2 M sodium formate for NADH/malate and NAD^+/pyruvate crystals, respectively. The ATP/malate complex was crystallized against a reservoir solution composed of 100 mM MES (pH 6.0), 8%–10% (w/v) PEG 20,000, and 5% (v/v) MPD. Crystals appeared within a few days in the shape of thin plates. For cryoprotection, the crystals were transferred to a solution containing 35% (w/v) PEG 3350 and 5 mM fumarate and $MnCl_2$, together with other components of the corresponding reservoir, and flash-frozen in liquid propane for X-ray data collection at 100 K.

Data Collection and Processing

X-ray diffraction data sets of the crystals of m-NAD-ME in complex with NADH/malate (at 2.3 Å resolution) and NAD^+/pyruvate (2.1 Å resolution) were collected at the National Synchrotron Light Source (NSLS) beamline X4A. An X-ray diffraction data set on the complex with ATP/malate (2.3 Å resolution) was collected at the ComCAT (32-ID) beamline at the Advanced Photon Source (APS). All the crystals belong to space group C2. The diffraction images were processed with the HKL package (Table 1) (Otwinowski and Minor, 1997).

Structure Determination and Refinement

The crystals are isomorphous to that of m-NAD-ME in complex with NAD^+ and oxalate that we reported earlier, with a tetramer in the asymmetric unit (Yang et al., 2000b). The structure refinement was carried out with the program CNS (Brünger et al., 1998), and the atomic model was rebuilt against the $2F_o - F_c$ electron density map with the program O (Jones et al., 1991). The models for the cofactor and the substrate were built in after the initial refinement with the protein atoms only (Figure 2D). The refinement statistics are summarized in Table 1.

Acknowledgments

We thank Gerwald Jogl, Javed Khan, Hailong Zhang, and Reza Khayat for help with data collection at synchrotron radiation sources; Randy Abramowitz and Craig Ogata for access to the X4A beamline; Steve Wasserman and Kevin D'Amico for access to the 32-ID beamline; and W.W. Cleland and Paul Cook for helpful discussions. This research was supported by a grant (MCB-99-74700) from the National Science Foundation to L.T.

Received: May 19, 2003
Revised: June 2, 2003
Accepted: June 9, 2003
Published: September 2, 2003

References

Bhargava, G., Mui, S., Pav, S., Wu, H., Loeber, G., and Tong, L. (1999). Preliminary crystallographic studies of human mitochondrial $NAD(P)^+$-dependent malic enzyme. J. Struct. Biol. *127*, 72–75.

Brünger, A.T., Adams, P.D., Clore, G.M., DeLano, W.L., Gros, P., Grosse-Kunstleve, R.W., Jiang, J.-S., Kuszewski, J., Nilges, M., Pannu, N.S., et al. (1998). Crystallography and NMR System: a new software suite for macromolecular structure determination. Acta Crystallogr. D Biol. Crystallogr. *54*, 905–921.

Carson, M. (1987). Ribbon models of macromolecules. J. Mol. Graph. *5*, 103–106.

Chang, G.-G., Wang, J.-K., Huang, T.-M., Lee, H.-J., Chou, W.-Y., and Meng, C.-L. (1991). Purification and characterization of the cytosolic $NADP^+$-dependent malic enzyme from human breast cancer cell line. Eur. J. Biochem. *202*, 681–688.

Chou, W.-Y., Huang, S.-M., Liu, Y.H., and Chang, G.-G. (1994). Cloning and expression of pigeon liver cytosolic $NADP^+$-dependent malic enzyme cDNA and some of its abortive mutants. Arch. Biochem. Biophys. *310*, 158–166.

Cleland, W.W. (1999). Mechanisms of enzymatic oxidative decarboxylation. Acc. Chem. Res. *32*, 862–868.

Cleland, W.W. (2000). Chemical mechanism of malic enzyme as determined by isotope effects and alternate substrates. Protein Pept. Lett. *7*, 305–312.

Coleman, D.E., Rao, G.S., Goldsmith, E.J., Cook, P.F., and Harris, B.G. (2002). Crystal structure of the malic enzyme from Ascaris suum complexed with nicotinamide adenine dinucleotide at 2.3 Å resolution. Biochemistry *41*, 6928–6938.

Evans, S.V. (1993). SETOR: hardware lighted three-dimensional solid model representations of macromolecules. J. Mol. Graph. *11*, 134–138.

Hibberd, J.M., and Quick, W.P. (2002). Characteristics of C4 photosynthesis in stems and petioles of C3 flowering plants. Nature *415*, 451–454.

Hsu, R.Y., and Lardy, H.A. (1967). Pigeon liver malic enzyme. II. Isolation, crystallization, and some properties. J. Biol. Chem. *242*, 520–526.

Jones, T.A., Zou, J.Y., Cowan, S.W., and Kjeldgaard, M. (1991). Improved methods for building protein models in electron density maps and the location of errors in these models. Acta Crystallogr. A *47*, 110–119.

Karsten, W.E., Chooback, L., Liu, D., Hwang, C.-C., Lynch, C., and Cook, P.F. (1999). Mapping the active site topography of the NAD-malic enzyme via alanine-scanning site-directed mutagenesis. Biochemistry *38*, 10527–10532.

Kuo, C.-C., Tsai, L.-C., Chin, T.-Y., Chang, G.-G., and Chou, W.-Y. (2000). Lysine residues 162 and 340 are involved in the catalysis and coenzyme binding of NADP+-dependent malic enzyme from pigeon. Biochemistry Biophys. Res. Commun. *270*, 821–825.

Liu, D., Karsten, W.E., and Cook, P.F. (2000). Lysine 199 is the general acid in the NAD-malic enzyme reaction. Biochemistry *39*, 11955–11960.

Loeber, G., Infante, A.A., Maurer-Fogy, I., Krystek, E., and Dworkin, M.B. (1991). Human NAD^+-dependent mitochondrial malic enzyme. J. Biol. Chem. *266*, 3016–3021.

Loeber, G., Dworkin, M.B., Infante, A., and Ahorn, H. (1994a). Characterization of cytosolic malic enzyme in human tumor cells. FEBS Lett. *344*, 181–186.

Loeber, G., Maurer-Fogy, I., and Schwendenwein, R. (1994b). Purification, cDNA cloning and heterologous expression of the human mitochondrial $NADP^+$-dependent malic enzyme. Biochem. J. *304*, 687–692.

Long, J.J., Wang, J.-L., and Berry, J.O. (1994). Cloning and analysis of the C4 photosynthetic NAD-dependent malic enzyme of Amaranth mitochondria. J. Biol. Chem. *269*, 2827–2833.

Mallick, S., Harris, B.G., and Cook, P.F. (1991). Kinetic mechanism of NAD:malic enzyme from *Ascaris suum* in the direction of reductive carboxylation. J. Biol. Chem. *266*, 2732–2738.

McKeehan, W.L. (1982). Glycolysis, glutaminolysis and cell proliferation. Cell Biol. Int. Rep. *6*, 635–650.

Moreadith, R.W., and Lehninger, A.L. (1984). Purification, kinetic behavior, and regulation of $NAD(P)^+$ malic enzyme of tumor mitochondria. J. Biol. Chem. *259*, 6222–6227.

Ochoa, S., Mehler, A., and Kornberg, A. (1947). Reversible oxidative decarboxylation of malic acid. J. Biol. Chem. *167*, 871–872.

Otwinowski, Z., and Minor, W. (1997). Processing of X-ray diffraction data collected in oscillation mode. Methods Enzymol. *276*, 307–326.

Rao, G.S.J., Coleman, D.E., Kulkarni, G., Goldsmith, E.J., Cook, P.F., and Harris, B.G. (2000). NAD-malic enzyme from Ascaris suum: sequence and structural studies. Protein Pept. Lett. *7*, 297–304.

Wei, C.-H., Chou, W.-Y., and Chang, G.-G. (1995). Identification of Asp^{258} as the metal coordinate of pigeon liver malic enzyme by site-specific mutagenesis. Biochemistry *34*, 7949–7954.

Xu, Y., Bhargava, G., Wu, H., Loeber, G., and Tong, L. (1999). Crystal structure of human mitochondrial NAD(P)+-dependent malic enzyme: a new class of oxidative decarboxylases. Structure *7*, 877–889.

Yang, Z., and Tong, L. (2000). Structural studies of a human malic enzyme. Protein Pept. Lett. *7*, 287–296.

Yang, Z., Batra, R., Floyd, D.L., Hung, H.-C., Chang, G.-G., and Tong, L. (2000a). Potent and competitive inhibition of malic enzymes by lanthanide ions. Biochem. Biophys. Res. Commun. *274*, 440–444.

Yang, Z., Floyd, D.L., Loeber, G., and Tong, L. (2000b). Structure of a closed form of human malic enzyme and implications for catalytic mechanism. Nat. Struct. Biol. *7*, 251–257.

Yang, Z., Lanks, C.W., and Tong, L. (2002a). Molecular mechanism for the regulation of human mitochondrial NAD-dependent malic enzyme by fumarate and ATP. Structure *10*, 951–960.

Yang, Z., Zhang, H., Hung, H.-C., Kuo, C.-C., Tsai, L.-C., Yuan, H.S., Chou, W.-Y., Chang, G.-G., and Tong, L. (2002b). Structural studies of pigeon cytosolic NADP+-dependent malic enzyme. Protein Sci. *11*, 332–341.

Accession Numbers

The atomic coordinates for the three structures have been deposited in the Protein Data Bank under accession codes 1PJ2, 1PJ3, and 1PJ4.